JOC*Article*

Theoretical Study of the Addition Patterns of C_{60} Fluorination: $C_{60}F_n$ ($n = 1-60$)

Gregory Van Lier,[†,‡] Montserrat Cases,[§,‡] Christopher P. Ewels,[∥,⊥] Roger Taylor,[#] and Paul Geerlings*[,‡]

Unité de Physico-Chimie et de Physique des Matériaux (P.C.P.M.), Université catholique de Louvain (UCL), Place Croix du Sud, 1 (Boltzmann), B-1348 Louvain-la-Neuve, Belgium; Research Group of General Chemistry (ALGC), Vrije Universiteit Brussel (VUB), Pleinlaan 2, B-1050, Brussels, Belgium; Institut de Química Computacional and Departament de Química, Universitat de Girona, E-17071 Girona, Catalonia, Spain; Composite Systems and Materials Department (DMSC), ONERA BP72, 29 Avenue de la Division Leclerc, 92322 Chatillon, France; Laboratoire de Physique des Solides (LPS), Université Paris Sud, Batiment 510, 91405 Orsay, France; and Chemistry Department, University of Sussex, Falmer, Brighton BN1 9QJ, United Kingdom

pgeerlin@vub.ac.be

Received September 13, 2004

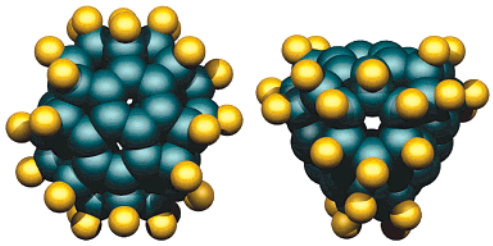

A systematic study is presented of addition patterns occurring upon fluorination of C_{60}. We use the program SACHA, which increments the number of fluorine addends, tests all available addition sites within a given cutoff radius, and selects the most energetically stable structure for further addition on the basis of full AM1 optimizations for every isomer. The lowest energy structures are optimized at HF/3-21G level of theory. A number of distinct addition routes are predicted, based on octahedral, '*S*', and '*T*' addition patterns, leading both to experimentally observed $C_{60}F_n$ isomers and to isomers not previously described in the literature. Furthermore the main addition routes were analyzed for $C_{60}F_{2n}$ isomers, using ab initio global and local aromaticity calculations. For this, magnetizability and NICS calculations have been carried out at HF/3-21G level of theory. We show the possibility of using NICS to predict the next preferential addition site, matching the above-described addition routes.

I. Introduction

In recent years, there has been a significant interest in fluorine derivatives of C_{60}. They are promising synthons as enhanced acceptors in donor−acceptor diads due to their specific characteristics (good solubility, high reactivity toward nucleophiles and enhanced dienophilicity of the unsubstituted part of the cage, resulting from electron withdrawal by fluorine atoms).[1,2]

Fluorine addition to C_{60} can be performed with a variety of agents.[3−12] The difficulty of controlling the

* To whom correspondence should be addressed. Phone: +32.2.629.33.14. Fax: +32.2.629.33.17.
[†] Université catholique de Louvain.
[‡] Vrije Universiteit Brussel.
[§] Universitat de Girona.
[∥] ONERA.
[⊥] Université Paris Sud.
[#] University of Sussex.

(1) Taylor, R. *Chem. Eur. J.* **2001**, *7*, 4074−4083.
(2) Taylor, R. *J. Fluorine Chem.* **2004**, *125*, 359−368.
(3) Boltalina, O. V.; Sidorov, L. N.; Bagryantsev, V. F.; Seredenko, V. A.; Zapol'skii, A. S.; Street, J. M.; Taylor, R. *J. Chem. Soc., Perkin Trans. 2* **1996**, 2275−2278.
(4) Hamwi, A.; Latouche, C.; Marchand, V.; Dupuis, J.; Benoit, R. *J. Phys. Chem. Solids* **1996**, *57*, 991−998.
(5) Tuinman, A. A.; Mukherjee, P.; Adcock, J. L.; Hettich, R. L.; Compton, R. N. *J. Phys. Chem.* **1992**, *96*, 7584−7589.
(6) Kniaz, K.; Fischer, J. E.; Selig, H.; Vaughan, G. B. M.; Romanow, W. J.; Cox, D. M.; Chowdhury, S. K.; McCauley, J. P.; Strongin, R. M.; Smith, A. B., III. *J. Am. Chem. Soc.* **1993**, *115*, 6060−6064.
(7) Boltalina, O. V.; Markov, V. Y.; Taylor, R.; Waugh, M. P. *Chem. Commun.* **1996**, 2549−2550.
(8) Neretin, I. S.; Lyssenko, K. A.; Antipin, M. Y.; Slovokhotov, Y. L.; Boltalina, O. V.; Troshin, P. A.; Lukonin, A. Y.; Sidorov, L. N.; Taylor, R. *Angew. Chem., Int. Ed.* **2000**, *39*, 3273−3276.
(9) Boltalina, O. V.; Borschevskii, A. Y.; Sidorov, L. N.; Street, J. M.; Taylor, R. *Chem. Commun.* **1996**, 529−530.

10.1021/jo0483872 CCC: $30.25
Published on Web 02/04/2005

reaction provides a complex mixture of products with varying numbers of fluorine atoms attached to the carbon cage and inhibits the isolation of the early compounds of fluorine addition. Nonetheless, many fluorofullerene derivatives have been characterized in recent years. Due to the specific reaction properties, higher fluorinated C_{60} derivatives were characterized initially ($C_{60}F_n$ with n = 18,[7] 20,[13,14] 36,[9] 48[12]), followed by lower fluorinated derivatives (n = 2,[15] and n = 4, 6, 8[16]) through further optimization of the reaction conditions (for an overview see ref 1). Study of these isolated species provides insight into the routes of addition followed and which systems play a key role in discriminating between distinct addition routes. Most of the fluorinations have been carried out using transition metal fluorides, as described generally.[17]

In general, fluorine addition to fullerenes presents two main features: the fluorine atoms are attached to the cage as fluorine pairs across 6,6-bonds, and the fluorination has a general tendency to create structures with increased aromaticity relative to the fullerene precursor and hence with increased stability.[18] In other words, the aromatic character of the fluorofullerenes increases with increasing number of fluorine atoms attached to the cage. Because fullerenes are moderately aromatic, addition of the first fluorine pair increases the localization of the electrons for the remaining double bonds of the two hexagons involved, so that further addition to these hexagons becomes thermodynamically favored.[16]

Similar features are found for hydrofullerenes, and comparisons between iso-structural $C_{60}X_n$ systems (X = H, F; n = 18,[19,20] 20,[14,21] 36[19]) suggest that the addition pattern follows a contiguous addition pathway, for which a 6,6-bond adjacent to an already functionalized bond is the preferential site for the next addition.[22,23] From the different hydrogen derivatives of C_{60} characterized at experimental level, two possible addition patterns have been proposed, the so-called '*S*' and '*T*' addition patterns (Figure 1).[20,24]

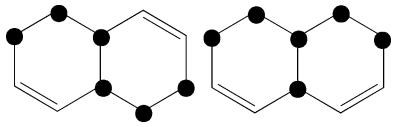

FIGURE 1. '*S*' and '*T*' addition patterns.

The first pair of fluorine atoms adds to a 6,6-bond, forming 1,2-$C_{60}F_2$. The second pair attaches to an adjacent 6,6-bond of the same hexagon, forming 1,2,3,4-$C_{60}F_4$. For the third pair two possibilities exist, depending on which adjacent 6,6-bond is chosen; either the first '*T*' or the first '*S*' isomer is formed (hereafter referred to as the '*T*'-$C_{60}F_6$ or '*S*'-$C_{60}F_6$ isomers). '*S*'-$C_{60}F_6$ has been isolated but '*T*'-$C_{60}F_6$ has not, attributed to the fact that it undergoes rapid further fluorination to form $C_{60}F_8$, which retains the '*T*' motif, although initially wrongly assigned due to anomalies in the ^{19}F NMR spectrum (see below).[16] Just as 1,2-addition in chlorination and bromination is predicted to be unfavorable compared to 1,4-addition, so for fluorination the converse is true[25] with only two examples of 1,4-addition being known. One involves a remote 1,4-addition to $C_{60}F_6$ giving $C_{60}F_8$;[16,26] the other concerns fluorodebromination of T_h-$C_{60}Br_{24}$ by a mechanism that is very unclear.[27]

Further fluorine addition to C_{60} following the '*T*' pattern yields $C_{60}F_{18}$. The most stable $C_{60}F_{18}$ isomer[7] was reported to have C_{3v} symmetry with a strongly distorted cage structure. All of the fluorine atoms are bound to one hemisphere of the C_{60} cage, which has a planar six-membered benzenoid ring surrounded by 18 sp^3 C atoms. The other hemisphere consists of 24 sp^2 C atoms, with a flattened equatorial belt of 12 sp^2 C atoms separating the two hemispheres. The isolation and characterization of $C_{60}F_{16}$, as part of the '*T*' addition path to $C_{60}F_{18}$, has been reported,[28] although this system may be formed upon fragmentation of $C_{120}F_{32}$ during mass spectrometry.[2]

The '*S*' pattern (also called the zigzag addition pattern) results in the formation of $C_{60}F_{20}$. Besides $C_{60}F_6$ itself this is the only '*S*' pattern isomer to be isolated and characterized. It was named *Saturnene* in view of its unique structure comprising flattened poles and an extended equator of sp^3 C atoms.[14]

Although theoretical studies have already been performed very early on fluorofullerenes,[25,29–31] these did not involve an analysis of the addition patterns. In this work we present a systematic analysis of the addition patterns governing the fluorination of C_{60} to form $C_{60}F_n$ (n = 1–60). For this we have developed the program SACHA that allows a systematic analysis of chemical addition by incrementing the number of addends, testing all available addition sites within a given surface distance cutoff radius, and using the most energetically stable

(10) Boltalina, O. V.; Street, J. M.; Taylor, R. *J. Chem. Soc., Perkin Trans. 2* **1998**, 649–654.
(11) Boltalina, O. V.; Buhl, M.; Khong, A.; Saunders: M.; Street, J. M.; Taylor, R. *J. Chem. Soc., Perkin Trans. 2* **1999**, 1475–1479.
(12) Gakh, A. A.; Tuinman, A. A.; Adcock, J. L.; Sachleben, R. A.; Compton, R. N. *J. Am. Chem. Soc.* **1994**, *116*, 819–20.
(13) Matsuzawa, N.; Fukunaga, T.; Dixon, D. A. *J. Phys. Chem.* **1992**, *96*, 10747–10756.
(14) Boltalina, O. V.; Markov, V. Y.; Troshin, P. A.; Darwish, A. D.; Street, J. M.; Taylor, R. *Angew. Chem., Int. Ed.* **2001**, *40*, 787–789.
(15) Boltalina, O. V.; Lukonin, A. Y.; Street, J. M.; Taylor, R. *Chem. Commun.* **2000**, 1601–1602.
(16) Boltalina, O. V.; Darwish, A. D.; Street, J. M.; Taylor, R.; Wei, X.-W. *J. Chem. Soc., Perkin Trans. 2* **2002**, 251–256.
(17) Boltalina, O. V.; Lukonin, A. Y.; Gorjunkov, A. A.; Pavlovich, V. K.; Rykov, A. N.; Seniavin, V. A.; Sidorov, L. V.; Taylor, R. *Recent Adv. Chem. Phys. Fullerenes and Relat. Mater. (Proc. Electrochem. Soc.)* **1997**, *97*, 257.
(18) Taylor, R. *Lecture Notes on Fullerene Chemistry: A Handbook for Chemists*; Imperial College Press: London, 1999.
(19) Jenkins, S.; Heggie, M. I.; Taylor, R. *J. Chem. Soc., Perkin Trans. 2* **2000**, 2415–2419.
(20) Darwish, A. D. M.; Avent, A. G.; Taylor, R.; Walton, S. R. M. *J. Chem. Soc., Perkin Trans 2* **1996**, 2051–2054.
(21) Clare, B. W.; Kepert, D. L. *J. Mol. Struct. (THEOCHEM)* **1994**, *315*, 71–83.
(22) Van Lier, G.; Safi, B.; Geerlings, P. *J. Chem. Soc., Perkin Trans. 2* **1998**, 349–354.
(23) van Lier, G.; De Proft, F.; Geerlings, P. *Phys. Solid State* **2002**, *44*, 588–592.
(24) Cahill, P. A. *Chem. Phys. Lett.* **1996**, *254*, 257–262.
(25) Dixon, D. A.; Matsuzawa, N.; Fukunaga, T.; Tebbe, F. N. *J. Phys. Chem.* **1992**, *96*, 6107–6110.
(26) Sandall, J. P. B.; Fowler, P. W. *Org. Biomol. Chem.* **2003**, *1*, 1061–1066.
(27) Denisenko, N. I.; Troyanov, S. I.; Popov, A. A.; Kuvychko, I. V.; Zemva, B.; Kemnitz, E.; Strauss, S. H.; Boltalina, O. V. *J. Am. Chem. Soc.* **2004**, *126*, 1618–1619.
(28) Avent, A. G.; Boltalina, O. V.; Lukonin, A. Y.; Street, J. M.; Taylor, R. *J. Chem. Soc., Perkin Trans. 2* **2000**, 1359–1361.
(29) Scuseria, G. E. *Chem. Phys. Lett.* **1991**, *176*, 423–427.
(30) Dunlap, B. I.; Brenner, D. W.; Mintmire, J. W.; Mowrey, R. C.; White, C. T. *J. Phys. Chem.* **1991**, *95*, 5763–5768.
(31) Bakowies, D.; Thiel, W. *Chem. Phys. Lett.* **1992**, *192*, 236–242.

structure for further addition, on the basis of full AM1 optimizations for every isomer and ab initio single-point calculations for the lowest energy isomers at HF/3-21G level of theory.[32] This study is compared with an ab initio analysis of the distinct members of each addition series found, based on geometrical, electronic, energetic and aromatic features. In accordance with previous studies,[23,33,34] an analysis of the relation between local aromaticity and the addition patterns is presented. The theoretical details are given in Section II and the results are discussed in Section III, where the first few addition products are analyzed separately (A), as they are the starting products of the distinct routes described (B to E), as well as the higher fluorination (F). General features of the reactivity toward fluorination and of the fluorinated products are given in the last part of Section III, before conclusions are drawn in the final section.

II. Theoretical and Computational Details

To systematically analyze addition patterns we have developed the program SACHA (Systematic Analysis of Chemical Addition),[32] which automates the process of generating isomers and geometry optimization. The method requires structural optimization of a large number of isomers and hence all optimization was performed with semiempirical AM1[35] using GAUSSIAN98[36] and GAUSSIAN03.[37] In this way it takes at most several hours to consider all isomers for a single fluorine addition. AM1 has been successfully applied for geometry optimizations in previous studies.[33,38] Full electron ab initio Hartree−Fock calculations were performed using the 3-21G basis set (HF/3-21G) for single-point energy calculations of given isomers (see below) as well as for all property calculations.

The methodology of SACHA is as follows: we take a given structure and seed it with a single addend followed by a structural relaxation. Different addends can be chosen for addition, consisting of a single atom (H, F, ...), an atom pair on neighboring atoms (H_2, F_2, ...), or a [1 + 2]-type addition (CR_2, NR, O, ...).[32] No symmetry is enforced during optimizations. For single atom addition, we then functionalize an additional carbon site, perform a full structural optimization, and store the energy. This is repeated for all possible addition sites for the new addend, within a surface distance cutoff radius defined in terms of the number of carbon neighbors between the C atom being considered for addition, and the nearest other functionalized carbon atom. The choice of surface distance cutoff radius is discussed below, as it can lead to different addition patterns, and may reflect for instance distant addition being more stable as compared to close range addition due to bulky addends or reactants.[18] The structure with the lowest energy is then taken as the base structure for addition of the next addend and the process repeated. For atom pair or [1 + 2]-type addition, a first addition site is chosen as above, the second addition site being one of the three sites neighboring the first. These three possible isomers are then treated separately.[32]

In this work, the fluorination of C_{60} is analyzed, so the most stable structure for $C_{60}F_n$ is taken as the structure to fluorinate to $C_{60}F_{n+1}$. This may not always be the case; for example, with F_2 gas addition it is possible that the first F adopts a less stable site in order to improve the energy gain with the second F. We therefore examined addition of a single fluorine atom at each step, as well as F_2 addition. Since both addition types were analyzed in conjunction, they will be discussed separately in the discussion below when appropriate.

Note that this method contains various restrictions. We do not take advantage of site symmetry at present. Fluorination is only allowed on the outer surface of the C_{60}. Since AM1 is spin-restricted, for single F addition the negative ions are considered for odd-numbers of fluorine ($C_{60}F_{2n+1}^-$), which prevents energetic comparison between odd- and even-numbered fluorinated systems but avoids the necessity of more time-consuming spin-unrestricted methods. Finally the method does not allow for fluorine rearrangement on the fullerene surface. This effect has been observed for high F coverage over extended periods of time at room temperature.[39] Despite these restrictions, the method is nonetheless shown to be valid for identifying the primary thermodynamically driven addition paths for fluorination.

Since the energies of the different isomers can be very close to each other, the energy ordering obtained from AM1 and HF/3-21G calculations with the same geometry do not always coincide. Therefore, predicting addition patterns based solely on AM1 can be inaccurate. However, a number of test calculations have shown that the same energy ordering was obtained from HF/3-21G calculated energies using AM1 geometries (commonly referred to as HF/3-21G//AM1) as from HF/3-21G optimized structures and HF/6-31G*//HF/3-21G calculations, and thus HF/3-21G//AM1 energies can be used reliably for predicting the lowest energy structure. AM1 energies are therefore determined for all isomers considered at a specific addition step, and HF/3-21G single-point energy calculations performed for those isomers with energies within 1 eV of the AM1 most stable isomer, defining the final order used to choose the most stable structure for further addition.

In cases where two isomers have very close energy, two or more systems were considered as a starting point for further addition, to examine the possible structural divergence at that point. (At these critical points of the distinct addition routes HF optimizations were performed, however only the HF/3-21G//AM1 energies are listed in the next section to maintain comparability, unless stated otherwise.) In total about 10 000 isomers were optimized at AM1 level in this way from $C_{60}F$ to

(32) Ewels, C. P.; Van Lier, G.; Geerlings P.; Charlier, J.-C. Manuscript in preparation.
(33) Van Lier, G.; Fowler, P. W.; De Proft, F.; Geerlings, P. *J. Phys. Chem. A* **2002**, *106*, 5128−5135.
(34) Van Lier, G.; De Proft, F.; Geerlings, P. *Chem. Phys. Lett.* **2002**, *366*, 311−320.
(35) Dewar, M. J. S.; Zoebisch, E. G.; Healy, E. F.; Stewart, J. J. P. *J. Am. Chem. Soc.* **1985**, *107*, 3902−3909.
(36) Frisch, M. J.; Trucks, G. W.; Schlegel, H. B.; Scuseria, G. E.; Robb, M. A.; Cheeseman, J. R.; Zakrzewski, V. G.; Montgomery Jr., J. A.; Stratmann, R. E.; Burant, J. C.; Dapprich, S.; Millam, J. M.; Daniels, A. D.; Kudin, K. N.; Strain, M. C.; Farkas, O.; Tomasi, J.; Barone, V.; Cossi, M.; Cammi, R.; Mennucci, B.; Pomelli, C.; Adamo, C.; Clifford, S.; Ochterski, J.; Petersson, G. A.; Ayala, P. Y.; Cui, Q.; Morokuma, K.; Malick, D. K.; Rabuck, A. D.; Raghavachari, K.; Foresman, J. B.; Cioslowski, J.; Ortiz, J. V.; Baboul, A. G.; Stefanov, B. B.; Liu, G.; Liashenko, A.; Piskorz, P.; Komaromi, I.; Gomperts, R.; Martin, R. L.; Fox, D. J.; Keith, T.; Al-Laham, M. A.; Peng, C. Y.; Nanayakkara, A.; Gonzalez, C.; Challacombe, M.; Gill, P. M. W.; Johnson, B. G.; Chen, W.; Wong, M. W.; Andres, J. L.; Head-Gordon, M.; Replogle, E. S.; Pople, J. A. *GAUSSIAN98*; Gaussian, Inc.: Pittsburgh, PA, 1998.
(37) Frisch, M. J.; Trucks, G. W.; Schlegel, H. B.; Scuseria, G. E.; Robb, M. A.; Cheeseman, J. R.; Montgomery, J. A.; Vreven, T.; Kudin, K. N.; Burant, J. C.; Millam, J. M.; Iyengar, S. S.; Tomasi, J.; Barone, V.; Mennucci, B.; Cossi, M.; Scalmani, G.; Rega, N.; Petersson, G. A.; Nakatsuji, H.; Hada, M.; Ehara, M.; Toyota, K.; R. Fukuda; J. Hasegawa; M. Ishida; T. Nakajima; Y. Honda; O. Kitao; H. Nakai; M. Klene; X. Li; J. E. Knox; H. P. Hratchian; J. B. Cross; C. Adamo; J. Jaramillo; R. Gomperts; R. E. Stratmann; O. Yazyev; A. J. Austin; R. Cammi; C. Pomelli; J. W. Ochterski; P. Y. Ayala; K. Morokuma; G. A. Voth; P. Salvador; J. J. Dannenberg; V. G. Zakrzewski; S. Dapprich; A. D. Daniels; M. C. Strain; O. Farkas; D. K. Malick; A. D. Rabuck; K. Raghavachari; J. B. Foresman; J. V. Ortiz; Q. Cui; A. G. Baboul; S. Clifford; J. Cioslowski; B. B. Stefanov; G. Liu; A. Liashenko; P. Piskorz; I. Komaromi; R. L. Martin; D. J. Fox; T. Keith; M. A. Al-Laham; C. Y. Peng; A. Nanayakkara; M. Challacombe; P. M. W. Gill; B. Johnson; W. Chen; M. W. Wong; C. Gonzalez; Pople, J. A. *GAUSSIAN03*; Gaussian, Inc.: Pittsburgh, PA, 2003.
(38) Cases Amat, M.; Van Lier, G.; Solà, M.; Duran, M.; Geerlings, P. *J. Org. Chem.* **2004**, *69*, 2374−2380.
(39) Avent, A. G.; Taylor, R. *Chem. Commun.* **2002**, 2726−2727.

$C_{60}F_{60}$, from which about 2000 single point calculations were performed at HF/3-21G level of theory. This corresponds to more than 10^7 seconds or more than 120 days of calculation time in total, making it one of the largest fullerene isomer studies to date at this level of theory.[40] The total scale of this study mainly determined the level of theory being chosen, providing accurate results for reasonable computation times.

From the HOMO−LUMO gap one can obtain the kinetic stability,[41−44] calculated as the HOMO−LUMO energy separation multiplied by the number of carbon atoms conjugated in the system studied (e.g., 58 for $C_{60}F_2$, 56 for $C_{60}F_4$, 54 for $C_{60}F_6$, etc). Also called the *T*-value in its original description, we will here maintain the nomenclature "kinetic stability" in order to distinguish from the described '*T*' addition pattern.

Reaction enthalpies are approximated as the energy difference [$E_R = E(C_{60}F_n) - E(C_{60}F_{n-2}) - E(F_2)$], providing a measure of the exothermicity of fluorination. Hereby only the even-numbered systems were considered to maintain comparability (see above).

The important role of aromaticity in fullerene and nanotube chemistry has already been established.[23,33,45] Global aromaticity in terms of the molecular magnetizability for each system is calculated using the CSGT method.[46] With this we analyze the relative aromaticity of products in the addition series and whether aromaticity is related to energetic stability.

The local aromaticity of a ring is described by its ability to support diamagnetic ring (i.e., diatropic) currents, which can be described by the nucleus-independent chemical shift or NICS.[47] In accordance to previous studies,[23,34] this shift is calculated at the geometrical ring centers for all five- and six-membered rings of the cage, determined by the nonweighted mean of ring atom coordinates, using the GIAO method.[48] (For a review of aromaticity descriptors in theoretical methods we refer to ref 49) This methodology was already successfully applied for the prediction of subsequent addition sites, being identified as the bond shared by the rings having NICS closest to zero.[23,34] Therefore it is again applied here where it can be validated by the extensive analysis performed using SACHA. Molecular magnetizabilities and NICS were calculated at the HF/3-21G//AM1 level of theory, using the GAUSSIAN98[36] and GAUSSIAN03[37] program. We note that density functional theory (DFT) does not provide systematically better NMR results than Hartree−Fock methods, since current functionals do not include magnetic field dependence. For nonfluorinated C_{60}, NICS for pentagon and hexagon rings are +5.1 and −6.8 ppm, respectively, calculated at the geometrical ring centers (HF/3-21G//AM1).

III. Results and Discussion

For ease of identification we prefix each structure with the first letter of the addition route of which it is part. Although this identification is only correct in a strict sense for the first members of a given route, it enables unambiguous identification of subsequent members of the same addition route. The numbering used throughout is depicted in Figure 2.[50] In the next subsections the different stages of fluorination and the distinct addition routes will be discussed, and general features determining the fluorination to C_{60} will be presented at the end of this section.

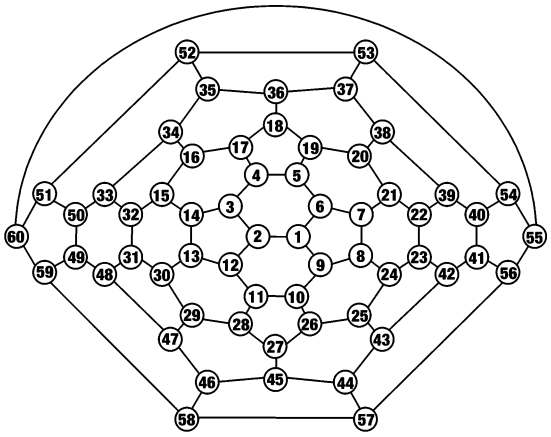

FIGURE 2. Numbering for the C atoms of C_{60} where F atoms are attached.[50]

For the systematic SACHA addition calculations it is necessary to determine a suitable surface distance cutoff radius for investigation, as this permits discrimination between different addition paths. The values chosen are given in the relevant sections below. It is also necessary to choose an energy cutoff, such that if an isomer has a formation energy higher than the ground state isomer plus this cutoff, we assume it will not form in sufficient quantity to act as a precursor for further addition routes. This isomer will therefore not be considered as a divergent route for fluorination. The energy cutoff used was arbitrarily chosen at 15 kcal/mol.

A. Early Additions: C_{60} to $C_{60}F_6$. In general, addition to C_{60} takes place at a 6,6-bond having a higher double bond character. This is also the case for fluorine addition, since 1,2-$C_{60}F_2$ is found to be 6.3 kcal/mol more stable than 1,4-$C_{60}F_2$. The 1,2-addition is also 24.7 kcal/mol more stable than 2,3-$C_{60}F_2$, mainly due to the additional strain occurring for addition to a pentagon. Nonetheless in the SACHA analysis, stepwise single F addition means that we still allow sampling of 5,6-bond addition isomers for completeness.

Further addition to 1,2-$C_{60}F_2$ leads to 1,2,3-$C_{60}F_3^-$ and 1,2,3,4-$C_{60}F_4$ as the most stable isomers, occurring at a 6,6-bond adjacent to the first added fluorine pair (the 6,6-bonds numbered 3,4-, 5,6-, 9,10-, or 11,12- are equivalent). The alternative octahedral addition yields 1,2,22,-23-$C_{60}F_4$ (or the equivalent 1,2,18,36-$C_{60}F_4$, 1,2,27,45-$C_{60}F_4$, or 1,2,31,32-$C_{60}F_4$). This isomer is a little less reactive (higher kinetic stability), has a higher magnetizability, and is 6.5 kcal/mol less stable than 1,2,3,4-$C_{60}F_4$. In Table 1, the total energy, band gap, kinetic stability and magnetizability are given for these systems. The results for C_{60} calculated at the same level of theory are given for reference. The selected systems are the most stable structures obtained from the previous addition

(40) Note: these calculations were performed on a cluster of 3 COMPAQ-DIGITAL AlphaServer GS Series (2 GS140 and 1 GS160) of the Computation Centre of the Free University of Brussels (VUB). Each GS140 server has six EV6.7 (700 MHz) CPUs and the GS160 server has 16 EV6.8CB (1001 MHz) CPUs, with an aggregate peak performance for the whole cluster of 48.80 Gflops.

(41) Aihara, J. *Theor. Chem. Acc.* **1999**, *102*, 134−138.
(42) Aihara, J.-I.; Oe, S. *Full. Sci. Technol.* **1999**, *7*, 871−878.
(43) Aihara, J.-i. *Phys. Chem. Chem. Phys.* **2000**, *2*, 3121−3125.
(44) Aihara, J. i.; Yoshida, M. *J. Mol. Graphics Modell.* **2001**, *19*, 194−198.
(45) Taylor, R. *Phys. Chem. Chem. Phys.* **2004**, *6*, 328−331.
(46) Cheeseman, J. R.; Trucks, G. W.; Keith, T. A.; Frisch, M. J. *J. Chem. Phys.* **1996**, *104*, 5497−5509.
(47) Schleyer, P. v. R.; Maerker, C.; Dransfeld, A.; Jiao, H.; van Eikema Hommes, N. J. R. *J. Am. Chem. Soc.* **1996**, *118*, 6317−6318.
(48) Wolinski, K.; Hinton, J. F.; Pulay, P. *J. Am. Chem. Soc.* **1990**, *112*, 8251−8260.
(49) De Proft, F.; Geerlings, P. *Chem. Rev.* **2001**, *101*, 1451−1464.
(50) Taylor, R. *J. Chem. Soc., Perkin Trans. 2* **1993**, 813−824.

TABLE 1. Total Energy (au), HOMO−LUMO Gap (au), Kinetic Stability (*T*-value in au), and Magnetizability χ (cgs-ppm) for Selected Systems

$C_{60}F_n$	fluorinated C	energy	band gap	kinetic stability	χ
C_{60}		−2259.0325	0.277	16.6	
$C_{60}F_2$	1,2	−2456.8228	0.267	15.5	−369
$C_{60}F_2$	2,3	−2456.7834	0.231	13.4	−342
$C_{60}F_2$	1,4	−2456.8128	0.268	15.6	−370
$C_{60}F_4$	1,2;3,4	−2654.6238	0.268	15.0	−397
'*O*'-$C_{60}F_4$	1,2;22,23	−2654.6134	0.269	15.1	−400
'*O*'-$C_{60}F_6$	27,45['*O*'-$C_{60}F_4$]	−2852.4054	0.294	15.9	−430
'*O*'-$C_{60}F_8$	31,32['*O*'-$C_{60}F_6$]	−3050.1931	0.291	15.1	−426
'*O*'-$C_{60}F_{10}$	18,36['*O*'-$C_{60}F_8$]	−3247.9800	0.281	14.0	−412
'*O*'-$C_{60}F_{12}$	55,60['*O*'-$C_{60}F_{10}$]	−3445.7670	0.282	13.5	−387
'*S*'-$C_{60}F_6$	1,2;3,4;9,10	−2852.4267	0.272	14.7	−425
'*S*'-$C_{60}F_8$	16,17['*S*'-$C_{60}F_6$]	−3050.2312	0.275	14.3	−455
'*S*'-$C_{60}F_{10}$	34,35['*S*'-$C_{60}F_8$]	−3248.0365	0.289	14.4	−488
'*S*'-$C_{60}F_{12}$	25,26['*S*'-$C_{60}F_{10}$]	−3445.8395	0.293	14.0	−501
'*S*'-$C_{60}F_{14}$	43,44['*S*'-$C_{60}F_{12}$]	−3643.6421	0.293	13.5	−515
'*S*'-$C_{60}F_{16}$	51,52['*S*'-$C_{60}F_{14}$]	−3841.4452	0.299	13.1	−529
'*S*'-$C_{60}F_{18}$	56,57['*S*'-$C_{60}F_{16}$]	−4039.2453	0.301	12.7	−549
'*S*'-$C_{60}F_{20}$	55,60['*S*'-$C_{60}F_{18}$]	−4237.0764	0.349	14.0	−571
'*T*'-$C_{60}F_6$	1,2;3,4;11,12	−2852.4207	0.269	14.5	−421
'*T*'-$C_{60}F_8$	28,29['*T*'-$C_{60}F_6$]	−3050.2256	0.280	14.6	−451
'*bis*'-$C_{60}F_8$	17,28['*T*'-$C_{60}F_6$]	−3050.1926	0.251	13.1	−444
'*T*'-$C_{60}F_{10}$	46,47['*T*'-$C_{60}F_8$]	−3248.0314	0.286	14.3	−481
'*bis*'-$C_{60}F_{10}$	16,29['*bis*'-$C_{60}F_8$]	−3248.0306	0.274	13.7	−461
'*T*'-$C_{60}F_{12}$	16,17['*T*'-$C_{60}F_{10}$]	−3445.8368	0.293	14.1	−492
'*bis*'-$C_{60}F_{12}$	48,49['*bis*'-$C_{60}F_{10}$]	−3445.8362	0.295	14.2	−489
'*T*'-$C_{60}F_{14}$	34,35['*T*'-$C_{60}F_{12}$]	−3643.6432	0.300	13.8	−504
'*bis*'-$C_{60}F_{14}$	33,50['*bis*'-$C_{60}F_{12}$]	−3643.6429	0.298	13.7	−499
'*T*'-$C_{60}F_{16}$	33,50['*T*'-$C_{60}F_{14}$]	−3841.4457	0.301	13.3	−512
'*bis*'-$C_{60}F_{16}$	16,17['*bis*'-$C_{60}F_{14}$]	−3841.4652	0.299	13.2	−515
'*T*'-$C_{60}F_{18}$	48,49['*T*'-$C_{60}F_{16}$]	−4039.2932	0.321	13.5	−530
'*C*'-$C_{60}F_{16}$	51,52['*C*'-$C_{60}F_{14}$]	−3841.4473	0.301	13.2	−517
'*C*'-$C_{60}F_{18}$	58,59['*C*'-$C_{60}F_{16}$]	−4039.2565	0.314	13.2	−536
'*C*'-$C_{60}F_{20}$	55,60['*C*'-$C_{60}F_{18}$]	−4237.0738	0.320	12.8	−552
$C_{60}F_{36}$	*T* symmetry	−5819.5097	0.420	10.1	−641
$C_{60}F_{48}$	C_1 symmetry	−7005.8257	0.426	5.1	

within a given addition route and will further be discussed below.

For the addition of a third pair of fluorine atoms different possibilities exist. In the case of octahedral addition, the next isomer will be 1,2,22,23,27,45-$C_{60}F_6$, leading to further octahedral addition (see Section B below.). Starting from 1,2,3,4-$C_{60}F_4$, different possibilities exist for $C_{60}F_5^-$. The lowest energy isomer 1,2,3,4,9-$C_{60}F_5^-$ leads to the '*S*' addition pattern upon further fluorination (see Section C and Figure 3c). However with an energy difference of only 2 kcal/mol, the 1,2,3,4,11-$C_{60}F_5^-$ isomer is found as the starting point of the '*T*'-addition pattern (see Section D and Figure 3d). Fluorination in these cases takes place at an adjacent 6,6-bond of the previous addition site.

The local aromaticity, as predicted by NICS (see Figure 3), shows the rings with values closest to zero lie around the fluorinated bonds for 1,2,3,4-$C_{60}F_4$ (Figure 3b). This lower aromaticity (hexagons) or anti-aromaticity (pentagons) means they will be more reactive and thus more likely to be the next addition site. The only difference for achieving the '*T*' or the '*S*' addition pattern lies in the hexagonal ring just outside the pyracylenic unit already functionalized. The lowest NICS for the hexagon adjacent to the '*S*'-$C_{60}F_6$ addition site is −9.9 ppm, compared to −10.3 ppm for the site adjacent to the '*T*'-$C_{60}F_6$ addition. The former should therefore be preferred for further functionalization and thus indeed lead to the lower energy '*S*' structure (1,2,3,4,9,10-$C_{60}F_6$), the latter leading to the '*T*' structure for $C_{60}F_6$ (1,2,3,4,11,12-$C_{60}F_6$).[24]

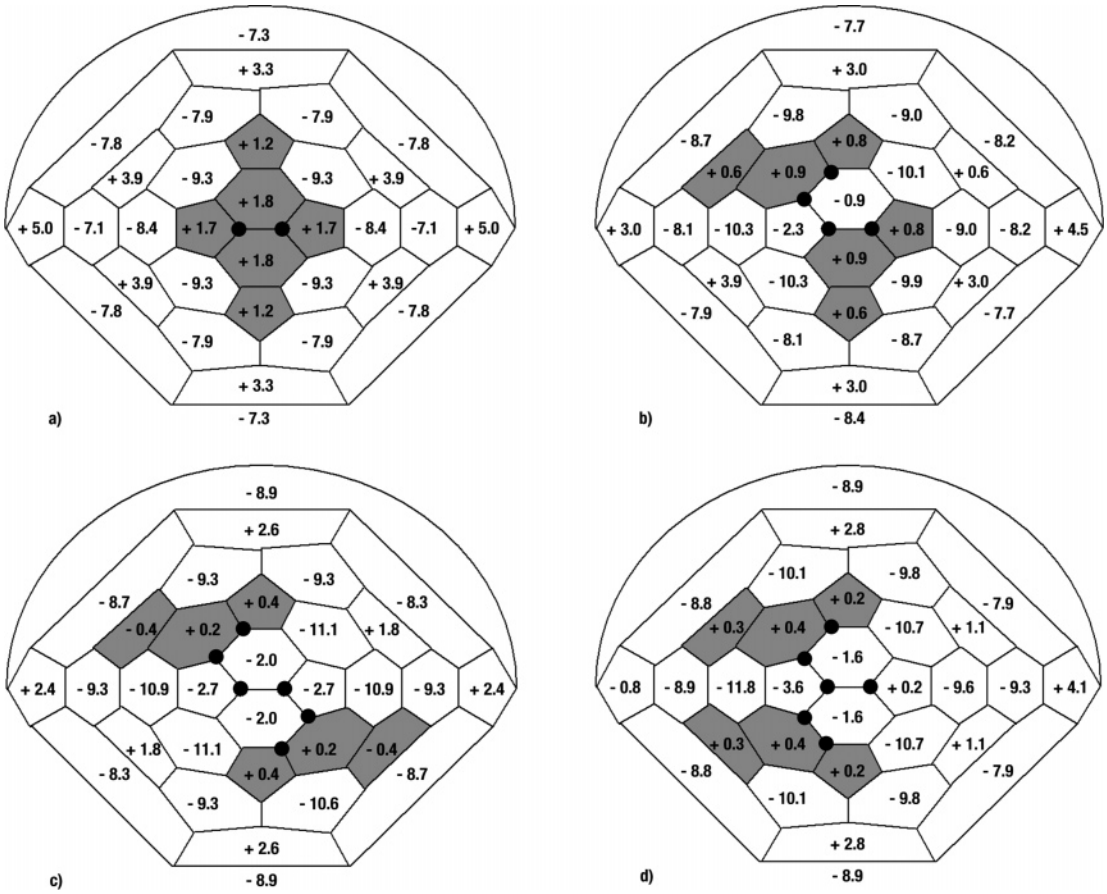

FIGURE 3. NICS for (a) $C_{60}F_2$, (b) $C_{60}F_4$, (c) '*S*'-$C_{60}F_6$, and (d) '*T*'-$C_{60}F_6$.

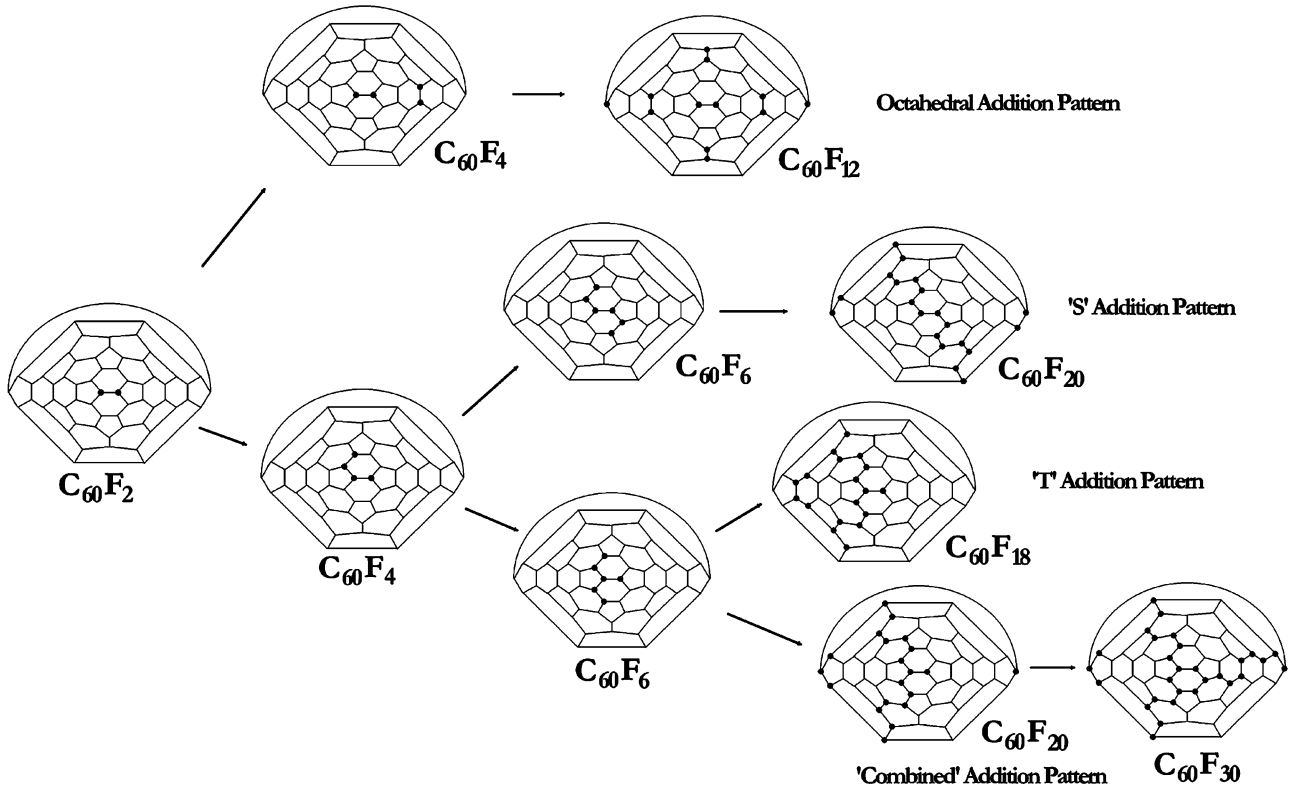

FIGURE 4. Overview of the distinct addition routes for fluorination to C_{60}.

Of these two most stable isomers of $C_{60}F_6$ (see Figure 3c and d), '*S*'-$C_{60}F_6$ is the most stable by 3.8 kcal/mol at HF/3-21G//AM1 and 4.1 kcal/mol at HF/3-21G//HF/3-21G. It is also the only one isolated experimentally.[16] Both isomers have a higher global aromaticity and kinetic stability than other $C_{60}F_6$ isomers. '*T*'-$C_{60}F_6$ may not be observed since it will undergo further fluorination at a higher rate than '*S*'-$C_{60}F_6$. If we compare reaction enthalpies, the value for '*T*'-$C_{60}F_8$ (+101.2 kcal/mol) is close to that for '*S*'-$C_{60}F_8$ (+100.9 kcal/mol), but the latter is more stable by 3.5 kcal/mol. So, '*T*'-$C_{60}F_6$ is more reactive as compared to '*S*'-$C_{60}F_6$, as is its reaction product '*T*'-$C_{60}F_8$.

We now consider four main addition routes to C_{60}, an overview of which is presented in Figure 4.

B. Octahedral Addition Pattern: $C_{60}F_6$ to $C_{60}F_{12}$. This first addition route is found when the surface distance cutoff radius was not restricted, i.e., all nonfunctionalized carbon atoms are considered as possible candidates for further functionalization, based on the AM1 energies. When running SACHA with these conditions, starting from the octahedral isomer for $C_{60}F_6$, an octahedral addition pattern is obtained, fluorine atoms adding in pairs at octahedral sites of the fullerene cage.[23] The hexakis adduct '*O*'-$C_{60}F_{12}$ consists of 12 fluorinated carbon atoms surrounding eight benzenoid rings of nonfluorinated carbon atoms. This addition pattern has previously been studied with local and global aromaticity descriptors for hydrogenation of C_{60}[23] and plays a more prominent role for bulky addends.[51]

Total energies, together with the band gap, the kinetic stability and magnetizabilities are given in Table 1, and the addition route is shown in Figure 5 where the fluorinated carbon atoms are numbered in order of addition. Although this addition pattern is predicted as the most stable at the AM1 level, HF/3-21G calculations show that for $C_{60}F_6$ to $C_{60}F_{12}$ more stable isomers exist at each addition step. '*O*'-$C_{60}F_6$ is 13.4 kcal/mol (9.6 kcal/mol) less stable than '*S*'-$C_{60}F_6$ ('*T*'-$C_{60}F_6$). When adding fluorine to an already fluorinated hexagon of $C_{60}F_8$ to $C_{60}F_{12}$ following a 1,2,3,4-addition pattern instead of at the octahedral site, isomers are typically more stable by 3 to 8 kcal/mol. These predictions show that it will be difficult to synthesize the octahedral isomers and explains why they have not been observed yet.

C. 'S' Addition Pattern: $C_{60}F_6$ to $C_{60}F_{20}$. When the surface distance cutoff was restricted so that only addition up to fourth neighbor of a fluorinated carbon was allowed, an addition pattern was obtained based on the '*S*' isomer for $C_{60}F_6$. Upon further functionalization of 1,2,3,4,9,10-$C_{60}F_6$, a zigzag addition pattern is found using SACHA, leading eventually to the stable $C_{60}F_{20}$ isomer, Saturnene.[14] Here, all fluorine atoms add to the equator of the cage, leaving two corannulene substructures unfluorinated (see Figure 6).

The addition pattern found with SACHA coincides with the predictions for the respective next preferential addition site based on the local aromaticity using NICS. For each next fluorofullerene derivative, the 6,6-bond predicted is again one for which the two C atoms are shared by one hexagon and two pentagons with NICS closest to zero.

From the calculated reaction enthalpies (see Figure 7), the formation of '*S*'-$C_{60}F_6$, '*S*'-$C_{60}F_8$ and '*S*'-$C_{60}F_{10}$ is increasingly exothermic, but for '*S*'-$C_{60}F_{12}$, '*S*'-$C_{60}F_{14}$ and

(51) Hirsch, A.; Vostrowsky, O. *Eur. J. Org. Chem.* **2001**, 829−848.

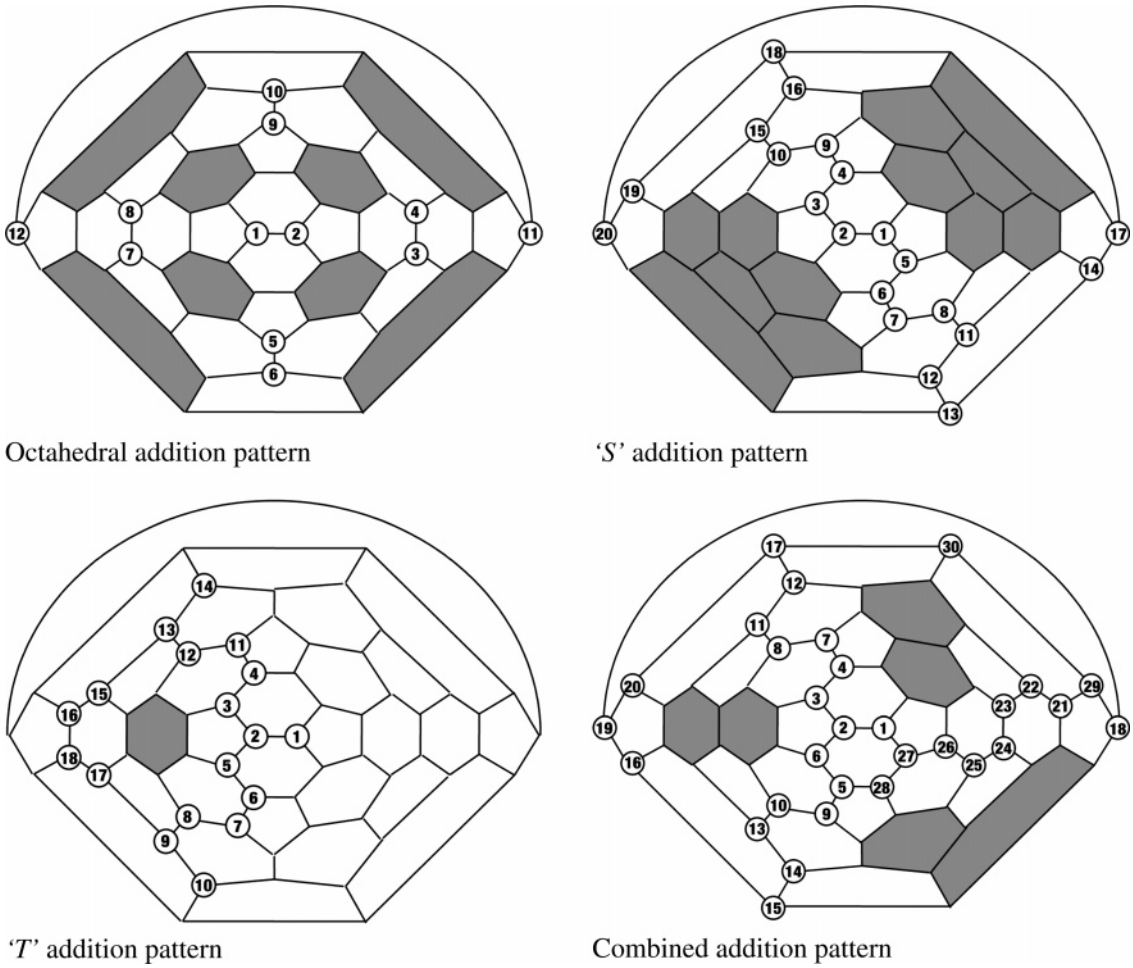

FIGURE 5. Overview of the different addition patterns considered, with distinct features shaded.

'*S*'-$C_{60}F_{16}$ it becomes less favorable until the formation of '*S*'-$C_{60}F_{18}$, which has the lowest exothermicity of all reactions of this '*S*'-series. The addition of two more fluorine atoms helps to stabilize the structure and so '*S*'-$C_{60}F_{20}$ becomes a favored reaction product, its high stability explaining the experimental isolation.[14] The values for the kinetic stability show a decreasing trend from '*S*'-$C_{60}F_6$ to '*S*'-$C_{60}F_{18}$, so they are predicted to be increasingly less stable and hence more reactive, coinciding with the fact that they have not yet been observed.

D. '*T*' Addition Pattern: $C_{60}F_6$ to $C_{60}F_{18}$. As mentioned above, a second isomer is found for $C_{60}F_5^-$, namely, 1,2,3,4,11-$C_{60}F_5^-$, which can be fluorinated to 1,2,3,4,11,-12-$C_{60}F_6$. Upon further fluorination, the lowest energy isomers are found when following a '*T*' addition pattern, surrounding an unfluorinated benzenoid ring. The order of addition is shown in Figure 8, leading to an experimentally observed $C_{60}F_{18}$ isomer with C_{3v} symmetry[7,20] and high aromaticity.[8,19] This isomer is also expected to be part of the functionalization route to the $C_{60}F_{36}$ isomer with *T* symmetry, as the fluorine motif of the former is present in the latter and they both form under the same conditions.[2,10] Local aromaticity of '*T*'-$C_{60}F_6$ again predicts addition at the 6,6-bond between atoms 16 and 17 (or the equivalent 28 and 29).

The structure thus predicted for '*T*'-$C_{60}F_8$ by both SACHA and the analysis of NICS is the '*T*'-$C_{60}F_8$ isomer depicted in Figure 8b. A different isomer was proposed for $C_{60}F_8$ in the literature, labeled '*bis*'-$C_{60}F_8$ in Table 1 (see Figure 8a).[16] This latter isomer is however less stable by 20.7 kcal/mol, as well as more reactive as predicted by the kinetic stability. The global aromaticity is also lower for this isomer, further explaining its lower stability. Thus we suggest it would be difficult to experimentally isolate this structure and that '*bis*'-$C_{60}F_8$ was not the structure isolated originally. Other isomers have more recently been proposed for the isolated $C_{60}F_8$ structure,[26] which need not necessarily lie on the contiguous pathway to '*T*'-$C_{60}F_{18}$. It seems indeed more likely that an isomer lying on an addition route to a stable fluorinated species needs to be reasonably reactive toward further fluorination in order for the addition to continue, and will thus be a less likely candidate to be isolated. '*T*'-$C_{60}F_8$ as shown in Figure 8b is therefore retained as part of the addition route to '*T*'-$C_{60}F_{18}$.

We note that the '*T*'-$C_{60}F_{18}$ isomer could also be obtained from '*S*'-$C_{60}F_6$, by adding two more fluorine atoms in a '*T*' pattern instead of an '*S*' pattern, and thus obtaining '*T*'-$C_{60}F_8$ from '*S*'-$C_{60}F_6$. This seems indeed a better solution since the '*T*' isomer for $C_{60}F_8$ is only 3.5 kcal/mol less stable as the '*S*' isomer, while this difference is 3.8 kcal/mol for the respective $C_{60}F_6$ isomers (see Table 1). Nonetheless, since this difference is even smaller for the respective $C_{60}F_5$ isomers (2 kcal/mol; see above), the divergence is predicted to occur at that point, thus upon

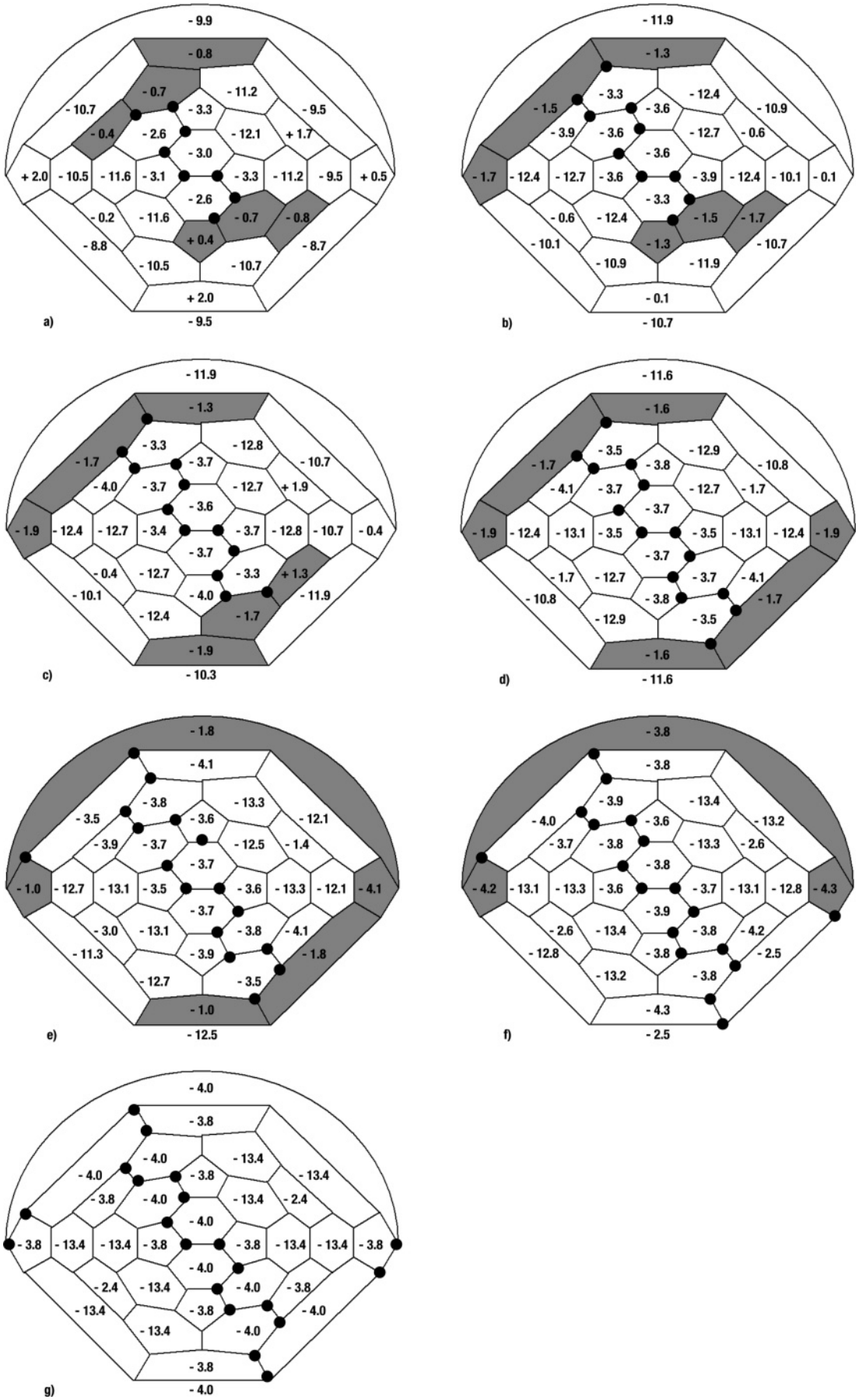

FIGURE 6. NICS for '*S*'-$C_{60}F_n$ (n = 8, 10, 12, 14, 16, 18, and 20).

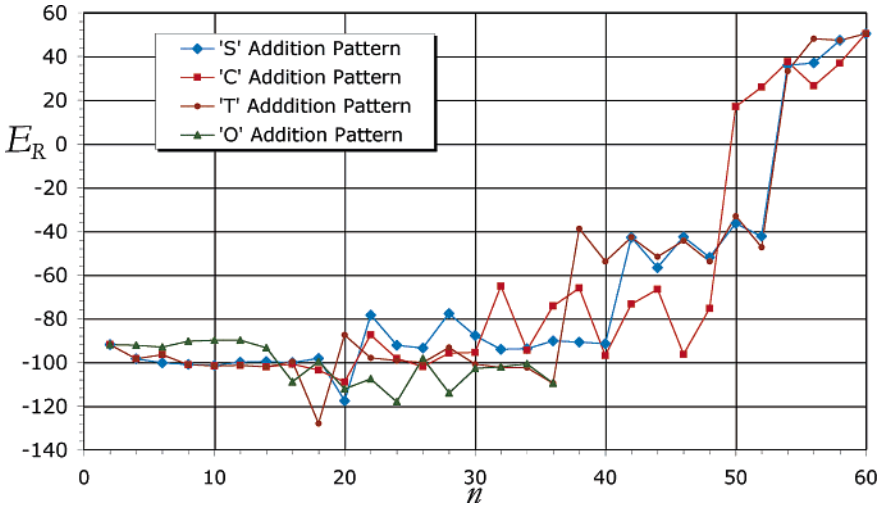

FIGURE 7. E_R in kcal/mol (HF/3-21G//AM1) versus the number n of fluorine atoms added. Since the values of E_R for the octahedral addition pattern are the same as for the '*T*' addition pattern for $n = 38-60$, they are omitted from the graph.

addition of the fifth fluorine atom, and so '*T*'-$C_{60}F_6$ is indeed believed to be a part of the addition route to '*T*'-$C_{60}F_{18}$.

From '*T*'-$C_{60}F_8$, further addition is predicted to give '*T*'-$C_{60}F_{10}$ (see Figure 8c). A second isomer could be obtained by adding two more fluorine atoms to carbons 16 and 17 (see Figure 8d), but this isomer, labeled '*bis*'-$C_{60}F_{10}$ since it could also be obtained from '*bis*'-$C_{60}F_8$, is less stable by 0.5 kcal/mol (see Table 1). The next member of the addition series predicted by NICS and obtained by SACHA from both isomers of $C_{60}F_{10}$ is the '*T*'-$C_{60}F_{12}$ isomer depicted in Figure 8e. The last two carbon atoms to be fluorinated in this case are numbered 16 and 17 from '*T*'-$C_{60}F_{10}$ or 46 and 47 from '*bis*'-$C_{60}F_{10}$. However, another isomer of $C_{60}F_{12}$ can be formed by fluorinating the atoms 48 and 49 from '*T*'-$C_{60}F_{10}$ (see Figure 8f). This isomer, labeled '*bis*'-$C_{60}F_{12}$, is less stable by 0.4 kcal/mol than '*T*'-$C_{60}F_{12}$, as well as less aromatic as predicted by the magnetizability (see Table 1). Although '*T*'-$C_{60}F_{10}$ and '*T*'-$C_{60}F_{12}$ are predicted to be the most stable intermediates, the '*bis*' isomers might also be synthesized upon continuous fluorination, given the small energy differences. But as these latter isomers are predicted to be more reactive than the respective '*T*' isomers, it will be difficult to isolate and hence characterize them. Both SACHA and the NICS pattern predict the next 6,6-bond of '*bis*'-$C_{60}F_{12}$ to be functionalized is 33,50 (or the equivalent 16,17-bond), giving '*bis*'-$C_{60}F_{14}$ as shown in Figure 8h. Following this analysis, from '*bis*'-$C_{60}F_{14}$ the '*bis*'-$C_{60}F_{16}$ structure (see Figure 8j) is predicted, which has been observed experimentally,[28] although it may be a dimer.[2]

Continued fluorination of '*T*'-$C_{60}F_{12}$ leads to '*T*'-$C_{60}F_{14}$ and '*T*'-$C_{60}F_{16}$ (see Figure 8g and 8i respectively). '*T*'-$C_{60}F_{14}$ is only 0.2 kcal/mol more stable than '*bis*'-$C_{60}F_{14}$. On the other hand, '*T*'-$C_{60}F_{16}$ is 12.2 kcal/mol less stable than '*bis*'-$C_{60}F_{16}$. Further fluorine addition gives '*T*'-$C_{60}F_{18}$ (Figure 8k), which corresponds to the experimentally isolated C_{3v} isomer predicted as the most stable of the different isomers for $C_{60}F_{18}$.[52] This structure has a fully delocalized benzenoid ring, with NICS of −13.7 ppm, surrounded with 18 fluorinated carbon atoms, resulting in a strongly distorted cage structure.

E. Combined Addition Pattern: $C_{60}F_6$ to $C_{60}F_{20}$. The '*T*' isomer of $C_{60}F_6$ (1,2,3,4,11,12-$C_{60}F_6$) can also lead to an alternative fluorination path to that described above. When fluorinating according to an '*S*' addition pattern after the initial 6 fluorine atoms are added, the addition follows the same path as the '*T*' addition pattern (see paragraph B.) until $C_{60}F_{14}$ but can then continue to form a $C_{60}F_{20}$ isomer where fluorinated carbon atoms now surround a naphthalenoid pattern instead of a benzenoid ring (see Figure 4). When '*T*'-$C_{60}F_{14}$ is further fluorinated, the most stable isomer is '*C*'-$C_{60}F_{16}$ (see Figure 9a), being 1.2 kcal/mol (10.9 kcal/mol) more stable than '*T*'-$C_{60}F_{16}$ ('*bis*'-$C_{60}F_{16}$) (see Table 1). Fluorination of '*C*'-$C_{60}F_{16}$ leads via '*C*'-$C_{60}F_{18}$ to the stable isomer '*C*'-$C_{60}F_{20}$, as depicted in Figure 9b and c, respectively, having a high global aromaticity due to the naphthalenoid center.

As these are the most stable isomers and since the global aromaticity is higher for the '*C*' isomers than the corresponding '*T*' isomers, this is a strong indication that these isomers would form under the same reaction conditions as '*T*'-$C_{60}F_{18}$. However, none of these isomers has been reported to date. A possible explanation for this is that the described '*bis*' isomers can be derived from the respective '*T*' isomers between '*T*'-$C_{60}F_8$ and '*T*'-$C_{60}F_{14}$, whereas in the opposite direction, only '*T*'-$C_{60}F_{16}$ is derived from a '*bis*' isomer (see Figure 10). The combination of the different paths and the respective reaction energies clearly point to the formation of '*T*'-$C_{60}F_{18}$, although it can be expected that intermediate '*T*' isomers may form at much lower concentration than the respective '*bis*' isomers.

In the same sense, this would predict even lower concentrations for the members of the combined addition route and could explain why they have not been observed yet. If synthesized, they are predicted to be present only in very small amounts, and discrimination of the distinct addition routes by tailoring the reaction conditions will be necessary to obtain these isomers.

(52) Clare, B. W.; Kepert, D. L. *J. Mol. Struct. (THEOCHEM)* **2003**, *621*, 211−231.

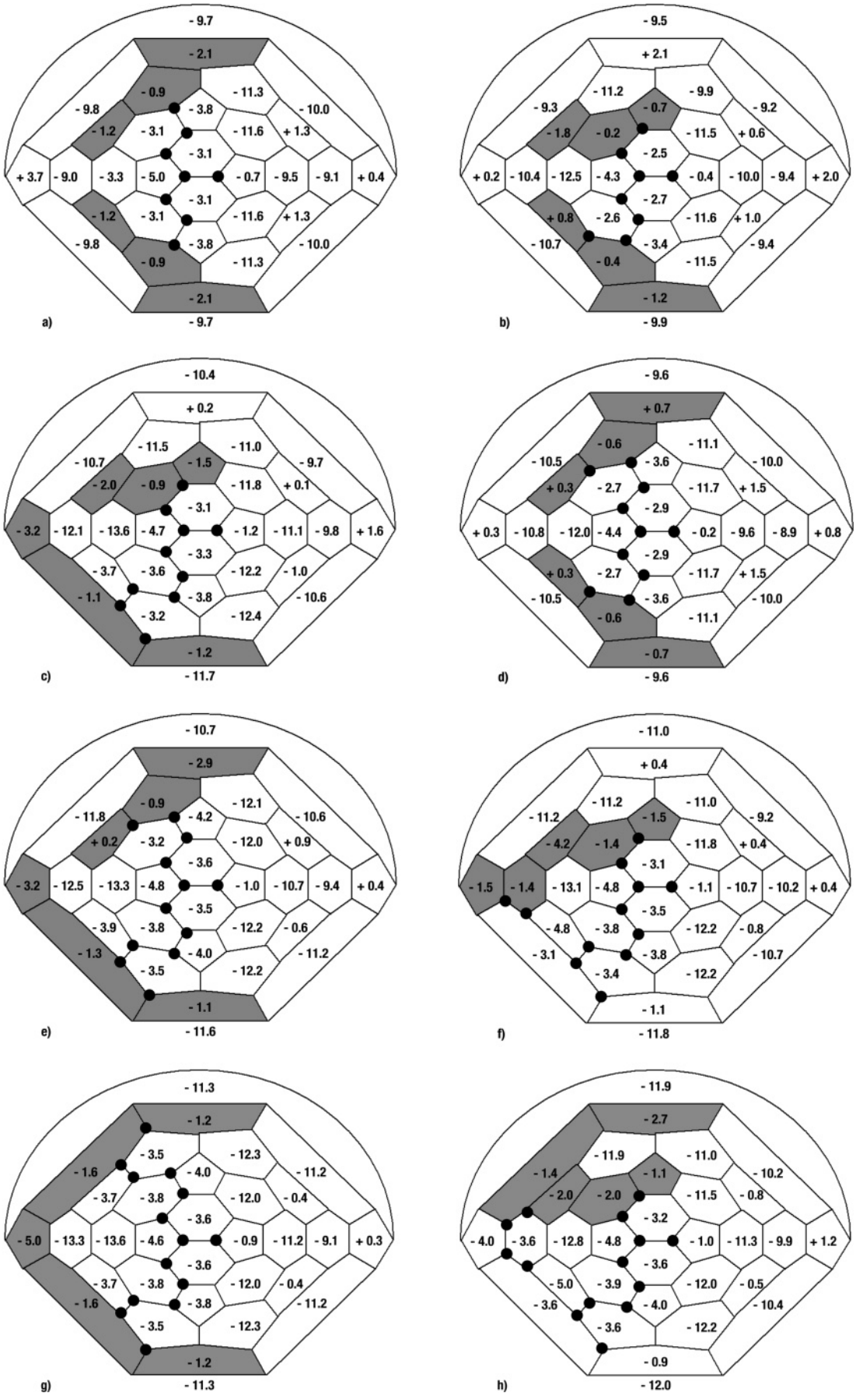
- 9.7
- 2.1
- 0.9
- 11.3
- 9.8
- 3.8
- 10.0
- 1.2
- 3.1
- 11.6
+ 1.3
- 3.1
+ 3.7
- 9.0
- 3.3
- 5.0
- 0.7
- 9.5
- 9.1
+ 0.4
- 3.1
- 1.2
- 3.1
- 11.6
+ 1.3
- 9.8
- 3.8
- 10.0
- 0.9
- 11.3
- 2.1
- 9.7
a)
- 9.5
+ 2.1
- 11.2
- 9.9
- 9.3
- 0.7
- 9.2
- 1.8
- 0.2
- 11.5
+ 0.6
- 2.5
+ 0.2
- 10.4
- 12.5
- 4.3
- 0.4
- 10.0
- 9.4
+ 2.0
- 2.7
+ 0.8
- 2.6
- 11.6
+ 1.0
- 10.7
- 3.4
- 9.4
- 0.4
- 11.5
- 1.2
- 9.9
b)
- 10.4
+ 0.2
- 11.5
- 11.0
- 10.7
- 1.5
- 9.7
- 2.0
- 0.9
- 11.8
+ 0.1
- 3.1
- 3.2
- 12.1
- 13.6
- 4.7
- 1.2
- 11.1
- 9.8
+ 1.6
- 3.3
- 3.7
- 3.6
- 12.2
- 1.0
- 1.1
- 3.8
- 10.6
- 3.2
- 12.4
- 1.2
- 11.7
c)
- 9.6
+ 0.7
- 0.6
- 11.1
- 10.5
- 3.6
- 10.0
+ 0.3
- 2.7
- 11.7
+ 1.5
- 2.9
+ 0.3
- 10.8
- 12.0
- 4.4
- 0.2
- 9.6
- 8.9
+ 0.8
- 2.9
+ 0.3
- 2.7
- 11.7
+ 1.5
- 10.5
- 3.6
- 10.0
- 0.6
- 11.1
- 0.7
- 9.6
d)
- 10.7
- 2.9
- 0.9
- 12.1
- 11.8
- 4.2
- 10.6
+ 0.2
- 3.2
- 12.0
+ 0.9
- 3.6
- 3.2
- 12.5
- 13.3
- 4.8
- 1.0
- 10.7
- 9.4
+ 0.4
- 3.5
- 3.9
- 3.8
- 12.2
- 0.6
- 1.3
- 4.0
- 11.2
- 3.5
- 12.2
- 1.1
- 11.6
e)
- 11.0
+ 0.4
- 11.2
- 11.0
- 11.2
- 1.5
- 9.2
- 4.2
- 1.4
- 11.8
+ 0.4
- 3.1
- 1.5
- 1.4
- 13.1
- 4.8
- 1.1
- 10.7
- 10.2
+ 0.4
- 3.5
- 4.8
- 3.8
- 12.2
- 0.8
- 3.1
- 3.8
- 10.7
- 3.4
- 12.2
- 1.1
- 11.8
f)
- 11.3
- 1.2
- 3.5
- 12.3
- 1.6
- 4.0
- 11.2
- 3.7
- 3.8
- 12.0
- 0.4
- 3.6
- 5.0
- 13.3
- 13.6
- 4.6
- 0.9
- 11.2
- 9.1
+ 0.3
- 3.6
- 3.7
- 3.8
- 12.0
- 0.4
- 1.6
- 3.8
- 11.2
- 3.5
- 12.3
- 1.2
- 11.3
g)
- 11.9
- 2.7
- 11.9
- 11.0
- 1.4
- 1.1
- 10.2
- 2.0
- 2.0
- 11.5
- 0.8
- 3.2
- 4.0
- 3.6
- 12.8
- 4.8
- 1.0
- 11.3
- 9.9
+ 1.2
- 3.6
- 5.0
- 3.9
- 12.0
- 0.5
- 3.6
- 4.0
- 10.4
- 3.6
- 12.2
- 0.9
- 12.0
h)

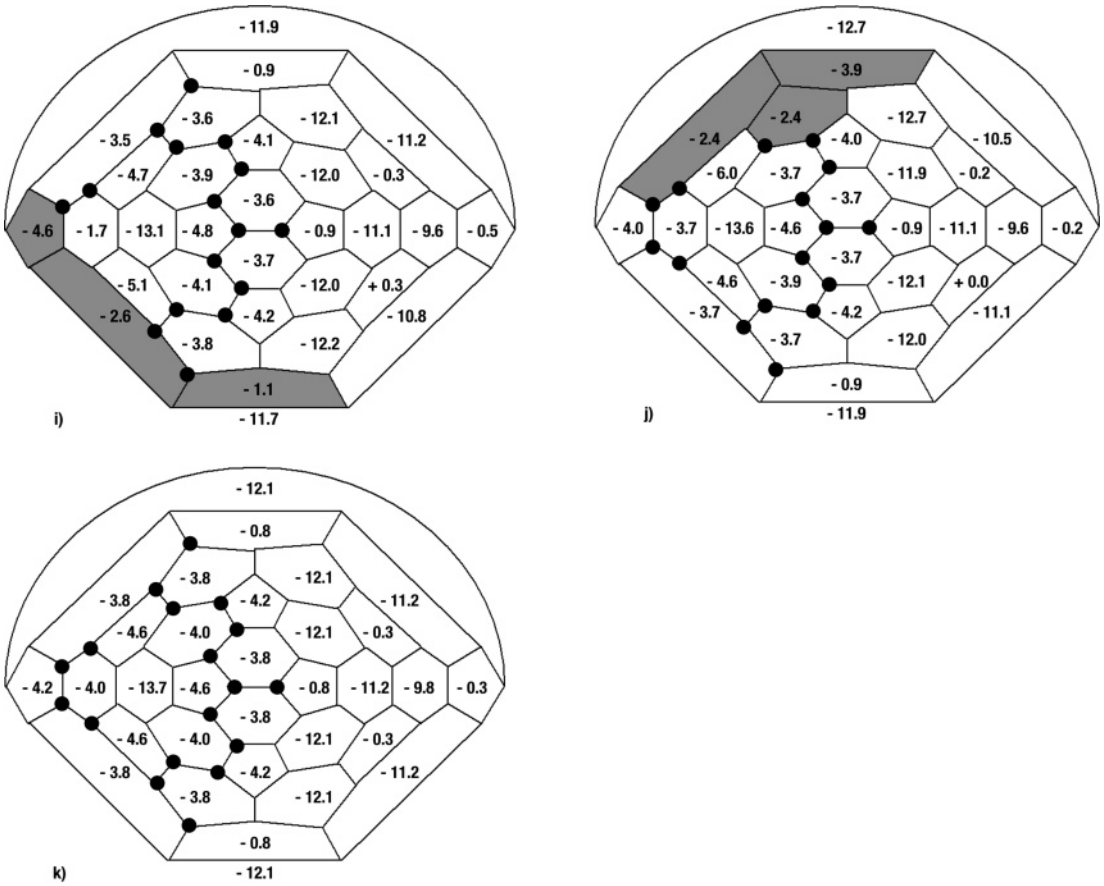

FIGURE 8. NICS for (a) '*bis*'-$C_{60}F_8$,[16] (b) '*T*'-$C_{60}F_8$, (c) '*T*'-$C_{60}F_{10}$, (d) '*bis*'-$C_{60}F_{10}$, (e) '*T*'-$C_{60}F_{12}$, (f) '*bis*'-$C_{60}F_{12}$, (g) '*T*'-$C_{60}F_{14}$, (h) '*bis*'-$C_{60}F_{14}$, (i) '*T*'-$C_{60}F_{16}$, (j) '*bis*'-$C_{60}F_{16}$, and (k) '*T*'-$C_{60}F_{18}$

F. Higher Fluorination to $C_{60}F_{60}$. The main isomers obtained following the '*T*', '*S*' and the combined '*C*' addition route, namely, '*T*'-$C_{60}F_{18}$, '*S*'-$C_{60}F_{20}$, and '*C*'-$C_{60}F_{20}$, all have a binding energy significantly higher than that of the isomers with less or more fluorine atoms on their respective routes. Nonetheless higher fluorination can be achieved, leading to stable structures.

Further addition to '*S*'-$C_{60}F_{20}$ will occur at one of the ten 6,6-bonds radiating from the top (or bottom) pentagon, since this isomer for '*S*'-$C_{60}F_{22}$ is more stable by 5.4 kcal/mol at HF/3-21G//HF/3-21G level of theory than the $C_{60}F_{22}$ formed by fluorinating one of the other ten 6,6-bonds, where a fully fluorinated hexagon would be formed.[53] The next two fluorine pairs are added at neighboring bonds radiating from the same pentagon, thus forming a '*T*' addition pattern on one of the hemispheres of '*S*'-$C_{60}F_{20}$. Putting the last fluorine pair at the other hemisphere is less stable by 17 kcal/mol, and forming an '*S*' addition pattern with a fully fluorinated hexagon by 10 kcal/mol. Fluorination at this one hemisphere continues until the formation of $C_{60}F_{30}$, followed by the same addition pattern at the other hemisphere giving $C_{60}F_{40}$. Exothermicities remain relatively high until the formation of this $C_{60}F_{40}$ isomer. Upon higher fluorination, E_R is typically half that for lower fluorination, showing the high strain this induces on the C_{60} cage. Similar binding energies are found for $C_{60}F_{44}$ and $C_{60}F_{48}$, and these highly fluorinated isomers could thus be obtained with the same reaction conditions. Fluorination is predicted to be exothermic until the formation of $C_{60}F_{52}$, and endothermic beyond (see Figure 7). $C_{60}F_{52}$ would thus be the highest fluorinated isomer obtainable upon exohedral addition following this addition path.

For the '*T*' addition pattern, further fluorination of '*T*'-$C_{60}F_{18}$ can occur at one of the hexagons neighboring the fluorinated belt (most stable), at the hexagon opposite the benzenoid ring (1.3 kcal/mol less stable), or at the benzenoid ring itself (58 kcal/mol less stable). Addition to a hexagon neighboring the equatorial belt (without providing a fully fluorinated hexagon), can occur at bond 8,24 (or the equivalent 37,38 -or 56,57-bond) or at bond 7,21 (or the equivalent 43,44- or 53,54-bond), which leads to two chiral $C_{60}F_{20}$ isomers. Fluorination can now occur at the two equivalent bonds. In this case, these three last fluorinated bonds form, together with three previously fluorinated bonds, an octahedral addition pattern. Further fluorination of '*O*'-$C_{60}F_{12}$ or '*T*'-$C_{60}F_{18}$ following this path is thus predicted to give the same isomer for $C_{60}F_{24}$. However, addition to the chiral $C_{60}F_{20}$ isomer at the hexagon opposite the benzenoid ring is more stable by 7.4 kcal/mol. Further addition will first surround a second benzenoid ring in $C_{60}F_{28}$, and then lead to the stable structure of $C_{60}F_{36}$ with *T* symmetry (see Figure 11a).[9−11] The same $C_{60}F_{36}$ will be obtained upon further fluorination of the octahedral addition pattern (in Figure 7, the values for E_R are therefore omitted beyond $C_{60}F_{38}$ for the octahedral addition pattern as they are the same as for

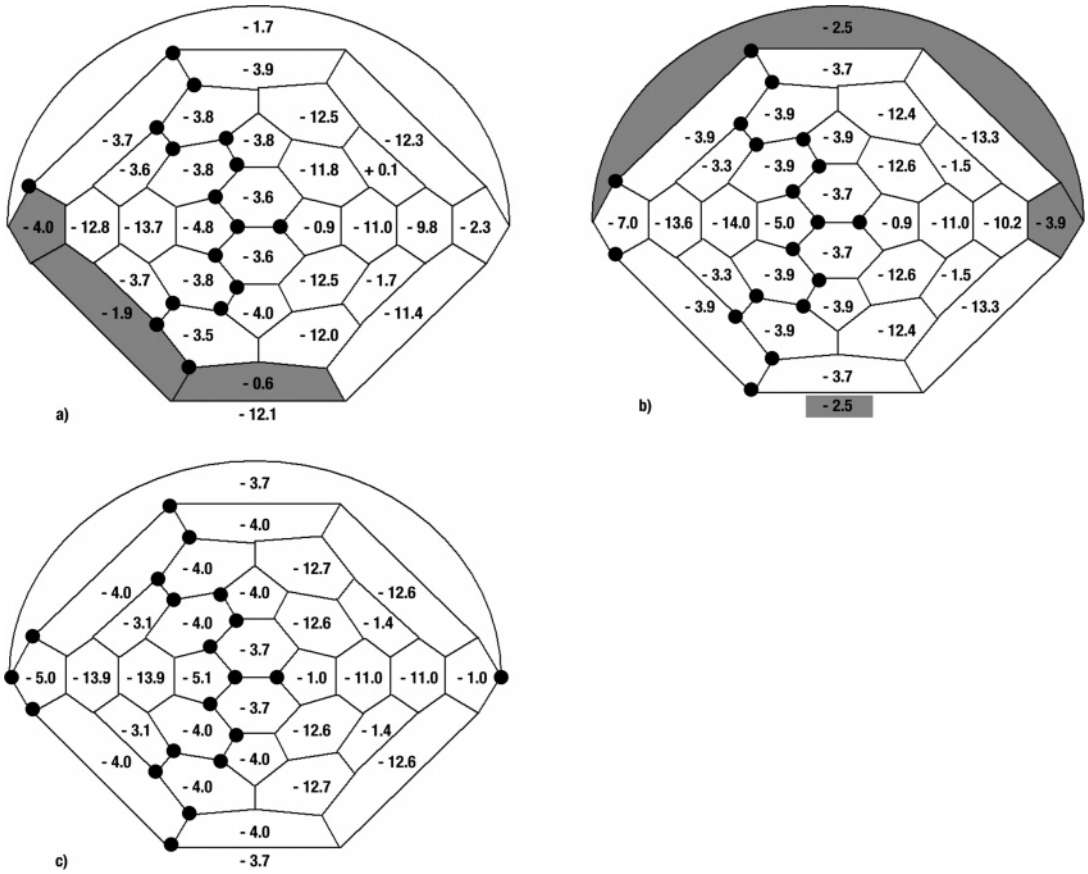

FIGURE 9. NICS for (a) '*C*'-$C_{60}F_{16}$, (b) '*C*'-$C_{60}F_{18}$, and (c) '*C*'-$C_{60}F_{20}$.

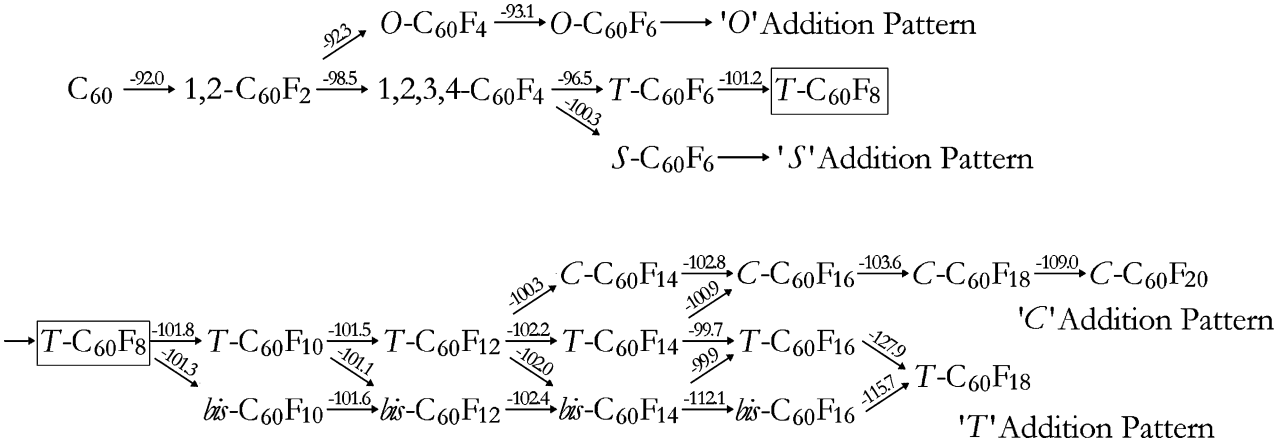

FIGURE 10. Overview of the addition routes with E_R (kcal/mol) indicated.

the '*T*' pattern). Besides this high-symmetry isomer, two other $C_{60}F_{36}$ isomers have been characterized with C_1 and C_3 symmetry.[10,39,54] Further fluorination of the *T* symmetry $C_{60}F_{36}$ isomer leads to an unreported $C_{60}F_{48}$ isomer, consisting of one unfluorinated benzenoid ring and three unfluorinated 5,6-bonds. For fluorination higher than $C_{60}F_{36}$, E_R is again typically half that for lower fluorination. Here, similar binding energies are found for $C_{60}F_{40}$, $C_{60}F_{44}$, $C_{60}F_{48}$, and $C_{60}F_{52}$. For and higher fluorinated isomers, reactions are again predicted endothermic (see Figure 7).

When '*C*'-$C_{60}F_{20}$ undergoes further fluorination, a new isomer of $C_{60}F_{30}$ is found with D_{3h} symmetry, containing two fully fluorinated hexagons at each side of the structure, connected by three strings of fluorinated carbon atoms following the '*S*' addition pattern (see Figure 5). In this way, three unfluorinated naphthalenoid centers are created, with high stability as a result. This '*C*'-$C_{60}F_{30}$ structure with D_{3h} symmetry is depicted as a hexagon-centered Schlegel diagram in Figure 11b. Following the discussion above, this isomer may be difficult

(53) Clare, B. W.; Kepert, D. L. *J. Mol. Struct.* **2003**, *622*, 185−280.
(54) Avent, A. G.; Clare, B. W.; Hitchcock, P. B.; Kepert, D. L.; Taylor, R. *Chem. Commun.* **2002**, 2370−2371.

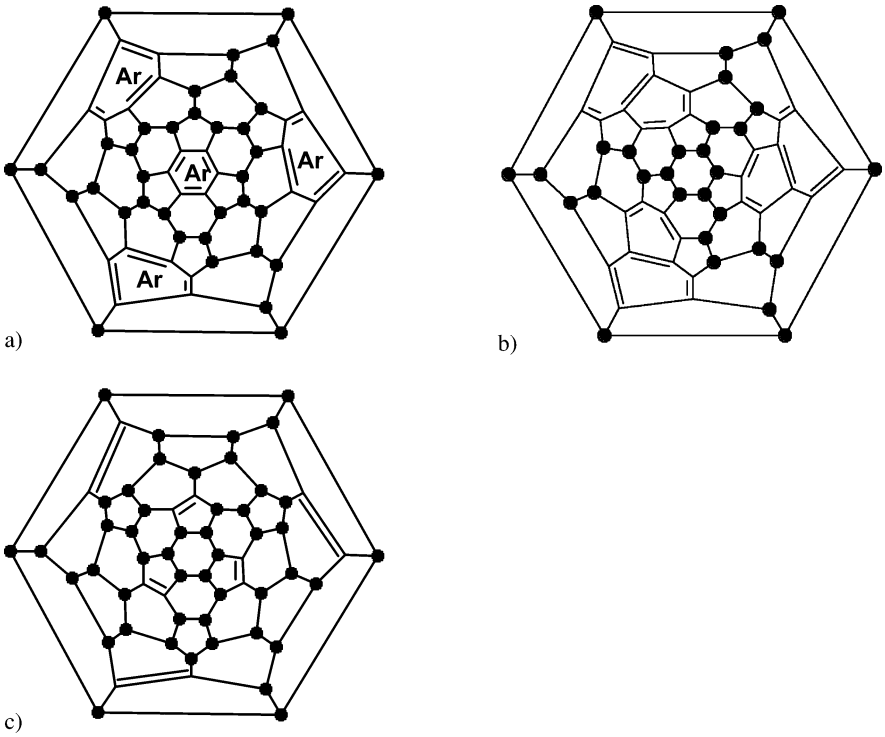

FIGURE 11. Hexagon-centered Schlegel diagrams for (a) $C_{60}F_{36}$ with *T* symmetry, (b) '*C*'-$C_{60}F_{30}$ with D_{3h} symmetry, and (c) the SS isomer of $C_{60}F_{48}$ with S_6 symmetry.

to isolate due to the fluorination reaction path C_{60} is expected to follow.

Continued fluorination of '*C*'-$C_{60}F_{30}$ fills in the naphthalenoid rings from the center outward (at one stage requiring 1,4 addition across a hexagon), resulting in each of the naphthalenoid centers having their two opposite 5,6-bonds unfluorinated. This leads to a chiral $C_{60}F_{48}$ structure with S_6 symmetry (see Figure 11c).[12] '*C*'-$C_{60}F_{30}$ may therefore form en route to this stable experimentally observed $C_{60}F_{48}$. Further addition to this $C_{60}F_{48}$ isomer is predicted endothermic (see Figure 7).

G. Further Interpretation and General Trends. From these results, a number of general trends can be formulated. First we observed a difference in stability between the octahedral and other addition patterns depending on whether we allowed single or pairwise F addition to the fullerene. Pairwise addition favors octahedral type additions whereas single F addition favors '*S*'- and '*T*'-type addition. In addition from the graph showing binding energy with each addition (Figure 7) it is clear than the octahedral addition route is smoother than the others, showing very few strong local minima. We suggest that octahedral addition may be favored for F_2 addition, for example, gas-phase fluorination, whereas the other routes will be favored in synthesis allowing single F addition.

The fluorination reactions described are all predicted to be highly exothermic up to relatively high fluorination addition. This exothermicity is also seen to increase upon increasing fluorination until a system with high stability is obtained. This shows the driving force of these reactions and can explain why $C_{60}F_2$ and other lower fluorofullerenes have only recently been isolated and characterized.[15,16]

Analysis of the geometries shows that the C−C bond length of fluorinated 6,6-bonds range from 1.62 to 1.58 Å with increasing number of fluorine atoms added, showing a higher double bond character (the experimental bond lengths for C_{60} are 1.458 Å for a 5,6-bond (60 bonds) and 1.401 Å for a 6,6-bond (30 bonds)[55] and are, respectively, 1.464 and 1.385 Å at the AM1 level of theory). The difference in bond length with C_{60} shows the distortion of the cage induced by fluorination. When we use NICS as a criterion to predict the preferential 6,6-bond for further fluorination, this is in all cases also the shortest 6,6-bond (corresponding to a higher double bound character) close to the previous one fluorinated, with a bond length of 1.367 Å or more. The shortening of these bonds also helps to explain the higher double bond character. In terms of the aromaticity analysis, we find the geometric and magnetic criteria to be in agreement.

As local aromaticity is expected to provide an indication of the addition route for subsequent addition (see previous fullerene hydrogenation studies),[23,34] it might be expected that the most aromatic isomer would be found upon each addition. To analyze this, a number of methods are possible. First, the global aromaticity could be used, as predicted by the magnetizability and/or the HOMO−LUMO gap. Also the kinetic stability should act as an indicator. A summation over the NICS values should also give an indication of the global aromaticity, as here the different contributions from the local ring currents should be taken into account. The question remains however whether a global sum over all NICS should be considered, or if one should take into account the conjugation of the system. In other words, it is possible that a less homo-

(55) Hedberg, K.; Hedberg, L.; Bethune, D. S.; Brown, C. A.; Dorn, H. C.; Johnson, R. D.; De Vries, M. *Nature* **1991**, *254*, 410−412.

geneous distribution of aromaticity is preferred. A clear correspondence is seen from the results between the general summation of NICS and the global aromaticity as predicted by the magnetizability. Global aromaticity as predicted by magnetizability and the HOMO−LUMO gap generally follows the same trend. In a number of cases discrepancies are seen, but in general the kinetically most stable system also shows the highest magnetizability, and is thus the less reactive isomer with a larger HOMO−LUMO gap (see Table 1).

NICS can provide further interpretation of the addition patterns observed. The electron deficiency of C_{60}, introduced by the pentagons in the structure as compared to graphene, is indeed seen to play a crucial role in the addition patterns followed. From the observation that the '*S*' pattern yields more stable structures than the '*T*' pattern (see Table 1), we note that for '*S*' patterns pentagons are created with two radiating bonds functionalized, whereas for '*T*' patterns three fluorinated radiating bonds per pentagon are created. From this, some general features can be discerned. If one of the radiating bonds of a pentagon is already functionalized, a second radiating bond, neighboring the first, is likely to be the next addition site, with this further increasing the diatropic character of this pentagon, as predicted by NICS. Adding a third addend pair on one of the radiating bonds of this pentagon does not provide important stability increase, but will always occur on a bond neighboring the first two, as addition to the opposite bond will lead to a less stable structure. A fully fluorinated hexagon is also seen to be disfavored. These general features are shown by the preference for the '*S*' over the '*T*' pattern, as for example for the addition route to '*C*'-$C_{60}F_{30}$.

Throughout this study, two distinct methodologies were followed, namely, systematic analysis using the newly developed program SACHA,[32] where a large number of isomers are considered for each number of addends and the energetically most stable isomer is considered for further addition (thermodynamic criteria), as well as the use of NICS or local aromaticity criteria to predict addition sites. The correspondence between these two shows that the use of NICS is a powerful tool for analyzing the reactivity of fullerenes and nanotubes, since it enables prediction of the most stable addition product.

This study also shows that SACHA can be used to analyze addition routes in a more systematic way. It can now be applied to a broad range of systems with many different addends and can be used with a number of quantum chemical codes allowing any level of theory required.[32] It can show distinct routes to form a given product, without having to analyze the enormous amount of isomers that can be conceived for this type of carbon cages. The program SACHA is also under further development in order to include other addition types and addends, to use different codes, and to restrict the number of isomers needing to be considered by taking advantage of symmetry. Also the possibility of alternative routes and the possibility of atom migration will be automated in future development[32]

IV. Conclusion

A systematic analysis of the addition patterns occurring for fluorination of C_{60} has been performed. A new program, SACHA, was developed that automatically generates and tests isomer structures, choosing the most stable as the basis for further addend addition. This is repeated, enabling a given addition route to be followed. The choice of a specific surface distance cutoff can be used to discriminate between different addition patterns. This methodology is currently used to investigate addition patterns during functionalization of higher fullerenes and carbon nanotubes, as well as the addition to structural defects.

From this analysis, four main addition routes were found, namely, an octahedral addition pattern, a '*T*'-shaped or an '*S*'- shaped addition pattern, and a combination of these last two (the '*C*' addition route). The octahedral route diverges from the others at $C_{60}F_2$ and leads to a stable $C_{60}F_{12}$ isomer; however, its intermediate $C_{60}F_4$ is less stable than the $C_{60}F_4$ isomer occurring in the '*S*' and '*T*' route. The '*S*' route proceeds by circumferential addition of F, leading to the stable Saturnene structure $C_{60}F_{20}$. An alternative, less stable and less aromatic $C_{60}F_6$ isomer leads to the '*T*' addition route, resulting in stable $C_{60}F_{18}$. At $C_{60}F_{12}$ this '*T*' addition route can also split to give a $C_{60}F_{16}$ containing a naphthalenoid rather than benzenoid ring. This '*C*' addition route ultimately leads to a new stable isomer, $C_{60}F_{30}$, not previously reported, having D_{3h} symmetry and three unfluorinated naphthalenoid substructures.

Further ab initio study of the '*T*' ($C_{60}F_n$ with $n = 2, 4, 6, ..., 18$) and '*S*' ($C_{60}F_n$ with $n = 2, 4, 6, ..., 20$) addition pattern, along with their local and global aromaticities, shows that '*S*'-$C_{60}F_n$ isomers are generally more aromatic than systems obtained from the '*T*' addition pattern.

Although different addition routes are described, discrimination of these distinct routes upon tailoring the reaction conditions will be necessary to obtain some of the isomers predicted. High fluorination is predicted to be exothermic until the formation of $C_{60}F_{48}$ for the '*C*' addition route and until $C_{60}F_{52}$ for the other addition routes.

Addition occurs at the most reactive bond. In a conjugated system such as C_{60}, this lies at the least delocalized site (NICS values more positive). This can be predicted by analyzing NICS of the rings surrounding a possible addition site and locating the bond surrounded by rings having NICS closest to zero. Our study showed that such bonds were the shortest nonfluorinated double bond in the system.

Subsequent addition occurs as long as systems are obtained with increasing aromaticity; this is seen as a driving force for the fluorination process. Global aromaticity, as predicted by the magnetizability of the system as well as by the HOMO−LUMO gap, therefore gives us an indication of the direction the addition is taking. Further indication of the addition pathway may come from the stability of the different isomeric reactions possible. Furthermore, the kinetic stability of the possible products can give an indication of relative stability and reactivity to further addition.

Acknowledgment. G.V.L. acknowledges the National Fund for Scientific Research (F.N.R.S.) for a

position as Scientific Research Worker. M.C. acknowledges support for this work by a travel grant and Ph.D. fellowship from the University of Girona. C.E. acknowledges the EU network COMELCAN and the EU Marie Curie fellowship scheme for funding. P.G. acknowledges the Fund for Scientific Research (FWO-Flanders) and the Free University of Brussels (VUB) for continuous support of his research group. C.E. and G.V.L. also thank Prof. Annick Loiseau for organizing the Ecole "Nanotubes: Science et Applications" where much of SACHA was developed, and we thank Prof. Jean-Christophe Charlier (UCL, Belgium) for valuable discussions.

Supporting Information Available: Optimized geometries in Cartesian coordinates of the AM1 optimizations for all structures discussed in detail and given in Table 1. This material is available free of charge via the Internet at http://pubs.acs.org.

JO0483872